Journal of Crystal Growth 584 (2022) 126574

Contents lists available at ScienceDirect

Journal of Crystal Growth

journal homepage: www.elsevier.com/locate/jcrysgro

Bandgap energy model for GaInNAsSb/GaAs alloys with high N content and strain influence

Riku Isoaho [a,*], Arto Aho [a], Antti Tukiainen [a], Turkka Salminen [b], Mircea Guina [a]

[a] Optoelectronics Research Centre, Physics Unit, Faculty of Engineering and Natural Sciences, Tampere University, P.O. Box 692, FI-33014 Tampere, Finland
[b] Tampere Microscopy Center, Tampere University, P.O. Box 692, FI-33014 Tampere, Finland

ARTICLE INFO

Communicated by Hajime Asahi

Keywords:
A1. Characterization
A3. Molecular beam epitaxy
B1. Antimonides
B1. Nitrides
B2. Semiconducting III-V materials

ABSTRACT

Bandgap energy of dilute nitride GaInNAsSb/GaAs alloys with N compositions as high as 8% are estimated using a method based on band anti-crossing model used for GaNAs/GaNSb/InNAs/InNSb ternary compounds. The parametrization of the model is defined by fitting with experimental composition and bandgap energy values employing a differential evolution algorithm. The effects of lattice strain on the bandgap energy are taken into account by the model resulting in an accurate prediction of the bandgap energy with an average deviation of only 12 meV compared to the experimental data. The model provides a useful tool for accurate determination of bandgap energies of dilute nitrides, including narrow bandgap, i.e. ~0.7 eV GaInNAsSb alloys, which are becoming increasingly relevant in the development of high-efficiency lattice-matched multijunction solar cells.

1. Main

Dilute nitrides are a class of compound semiconductors that formed by alloying small concentrations of N to the group V lattice sites in traditional III–V semiconductors [1,2]. Compared to other group V elements, N has a small atomic radius and high electronegativity, which have profound effects on the crystallographic, optical, and electrical properties of the dilute nitrides. Most notably, N incorporation drastically reduces the bandgap energy (E_g) of the host material and simultaneously reduces the lattice constant of the resulting crystal [2,3]. These features have been initially exploited in the development of GaInNAs/GaAs-based laser diodes at 1.3 μm range primary targeting uncooled operation [2,4–7]. More recently, the dilute nitrides have had a remarkable impact on the development of lattice-matched multijunction solar cells [8–11] owing to the fact that GaInNAsSb compounds with E_g from 1.4 eV down to 0.7 eV can be grown lattice-matched on GaAs and Ge substrates[2,8]. While the low N-content GaInNAsSb heterostructures with bandgaps of ~1 eV are well studied and the technology is rather mature, GaInNAsSb compounds with high N compositions exhibiting E_g around 0.7–0.8 eV require further technological and material science advances to be fully exploited in next-generation multijunction solar cells [12]. These developments are made possible by the use of molecular beam epitaxy (MBE), which enable a high degree of process control for N incorporation and significant reduction of N-related defects that is instrumental for device development [13,14].

Introduction of N to the crystal lattice is associated with formation of localized energy level near the conduction band edge of the host material. In turn, the interaction of these localized N-related resonant states with the conduction band of the host material leads to splitting of the conduction band into E_+ and E_- sub-bands, which effectively lowers the E_g of the material (i.e. now defined by the transition between E_- and valence bands) [15]. The reduction E_g in dilute nitride compounds is poorly described by the typical quadratic approximation [16]. Instead, the modification of conduction band structure due to N incorporation can be modelled with a so-called band anti-crossing (BAC) model [17]. Although, the effective use of BAC for GaInNAs has been widely established [18–21], there is a need for more advanced models for materials with higher N concentrations as well as for alloys with higher complexity incorporating also Sb.

Similar to N, incorporation of Sb also lowers the E_g yet this reduction takes place via the valence band structure instead of the conduction band [22]. Indeed, when N and Sb are incorporated simultaneously into GaAs or GaInAs, they affect both the valence and conduction bands [22]. For estimating the E_g of GaNAsSb alloys a double band anti-crossing (DBAC) model has been suggested [22]. Moreover, a relatively simple BAC-based model for GaInNAs has been tailored to estimate the E_g of GaInNAsSb alloys with N concentrations up to ~6% [23]. The adaptation to GaInNAsSb was based on using interpolated values of E_g for

* Corresponding author.
E-mail address: riku.isoaho@tuni.fi (R. Isoaho).

https://doi.org/10.1016/j.jcrysgro.2022.126574
Received 5 January 2022; Accepted 31 January 2022
Available online 4 February 2022

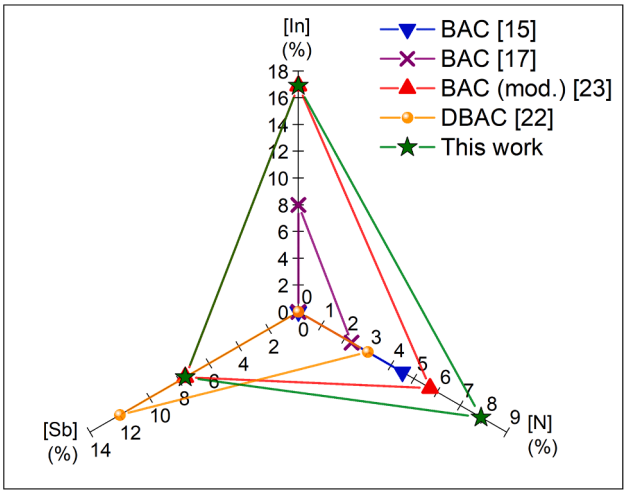

Fig. 1. Comparison of experimental composition ranges used for BAC-modelling of GaNAs, GaInNAs, GaInNAsSb and GaNAsSb reported in literature [15,17,22,23] along with the composition range reported in this work.

Table 1
Composition and bandgap data for the high N-content $Ga_{1-x}In_xN_yAs_{1-y-z}Sb_z$ samples used for the modelling. Values for alloys with lower N compositions are reported in Ref. [23].

	x	y	z	E_g (eV)
Sample A	0.147	0.057	0.003	0.862
Sample B	0.155	0.053	0.014	0.850
Sample C	0.160	0.060	0.018	0.796
Sample D	0.160	0.062	0.014	0.780
Sample E	0.163	0.079	0.009	0.727

GaInAsSb as the host material E_g in the BAC-model. This modified BAC-model yielded an excellent fit with the extensive experimental data but it ignored the effects of lattice strain; the model assumed that the deviation arising from residual strain was small within the data set. The modified BAC-model also showed slight drift between the modelled and experimental bandgap energies with higher In and N concentrations. In this paper, we propose an alternative interpolation scheme based on the BAC-model of N containing ternaries (i.e. GaNAs, GaNSb, InNAs and InNSb) for accurately predicting the E_g of GaInNAsSb/GaAs alloys, expanding the dataset to include low-bandgap materials, i.e. GaInNAsSb with up to 8 % N compositions. Fig. 1 shows the composition range covered by the proposed model, which is compared with compositions ranges of prior BAC-models used for modelling of dilute nitride alloys.

The modelling of E_g for $Ga_{1-x}In_xN_yAs_{1-y-z}Sb_z$ alloys starts from defining the material composition (x, y, z). As data points for model fitting we used the comprehensive composition and bandgap data presented by Aho *et al.* [23] together with additional compositions and E_g values for GaInNAsSb with higher N concentrations (i.e. bandgap energies down to ~0.7 eV). The compositions for these low-bandgap alloys (samples A-E; summarized in Table 1) were determined using energy-dispersive x-ray spectroscopy (EDS) measured from the cleaved facets of MBE-grown single-junction GaInNAsSb solar cells. The bandgap energies for these materials were extracted from external quantum efficiency (EQE) measurements made for the solar cells. Additional details on the EDS and EQE measurements for the high N-content solar cells can be found elsewhere [12].

Using the specified compositions, the lattice constant (a) for GaInNAsSb is approximated from lattice constants of binaries by using linear Vegard's law:

$$a_{GaInNAsSb} = x[ya_{InN} + za_{InSb} + (1-y-z)a_{InAs}] + (1-x)[ya_{GaN} + za_{GaSb} + (1-y-z)a_{GaAs}], \quad (1)$$

where the subscripts indicate the lattice constants of the binaries. Similar linear approximation is used to estimate the valence band hydrostatic deformation potential (a_V), conduction band hydrostatic deformation potential (a_C), elastic constants c_{11} and c_{12}, and the shear deformation potential (b_{ax}) for the GaInNAsSb material from the corresponding values of the binaries. The material parameters of the binaries used in this model are listed in Table 2.

The interpolated material parameters for GaInNAsSb are then used for estimating the influence of lattice strain on the band structure. The influence of hydrostatic strain component on the conduction band (CB) and valence band (VB) is given by [24]:

$$\delta E_{CB} = -2a_C\left(1-\frac{c_{12}}{c_{11}}\right)\varepsilon_{xx}, \quad (2)$$

$$\delta E_{VB} = -2a_V\left(1-\frac{c_{12}}{c_{11}}\right)\varepsilon_{xx}, \quad (3)$$

where ε_{xx} is the strain of the GaInNAsSb layer, which is defined by the lattice constants of the substrate (a_{subs}) and GaInNAsSb as $\varepsilon_{xx} = (a_{GaInNAsSb} - a_{subs})/a_{subs}$ [24]. The influence of the shear component of strain on the band structure is given by [24]:

$$\eta_{ax} = -2b_{ax}\left(1-2\frac{c_{12}}{c_{11}}\right)\varepsilon_{xx}. \quad (4)$$

The material parameters in Eqs. (2)–(4) are now the interpolated material parameters for GaInNAsSb. The hydrostatic strain components from Eqs. (2)–(3) and the shear strain component from Eq. (4) are used for estimating the strain-induced shifts for CB, and light-hole (LH) and heavy-hole (HH) bands [24]:

$$\Delta E_{CB} = \delta E_{CB}, \quad (5)$$

$$\Delta E_{LH} = \delta E_{VB} + \eta_{ax}, \quad (6)$$

$$\Delta E_{HH} = \delta E_{VB} - \eta_{ax}. \quad (7)$$

Using these, the total strain-induced shift of the E_g is approximated with:

$$\Delta E_g = \begin{cases} \Delta E_{CB} - \Delta E_{HH}, & \varepsilon_{xx} \geq 0 \\ \Delta E_{CB} - \Delta E_{LH}, & \varepsilon_{xx} < 0 \end{cases}. \quad (8)$$

Next, the BAC-model is used for estimating the E_g of the N-containing ternaries, i.e. GaNAs, GaNSb, InNAs and InNSb corresponding to E_- given by [17,25]:

Table 2
Material parameters for binaries [16,24].

	GaAs	GaSb	GaN	InAs	InSb	InN
a (Å)	5.6563	6.0959	4.5000	6.0583	6.4794	4.9800
a_C (eV)	−7.17	−7.50	−6.71	−5.08	−6.94	−2.65
a_V (eV)	−1.16	−0.80	−0.69	−1.00	−0.36	−0.70
c_{11} (GPa)	1221	884.2	293.0	832.9	684.7	187.0
c_{12} (GPa)	566.0	402.6	159.0	452.6	373.5	125.0
b_{ax} (eV)	−2.0	−2.0	−2.0	−1.8	−2.0	−1.2

Table 3
Bandgap energies of binaries at 300 K [16].

	GaAs	GaSb	InAs	InSb
E_g (eV)	1.4225	0.7267	0.3538	0.1737

Table 4
BAC parameters used in this work [18,23,26].

Ternary material	E_N (eV)	V_{MN} (eV)
GaNAs	1.65	2.55
GaNSb	0.78	2.60
InNAs	1.44	2.00
InNSb	0.65	3.00

$$E_{\pm} = \frac{1}{2}[E_M + E_N \pm \sqrt{(E_N - E_M)^2 + 4V_{MN}^2 y}], \quad (9)$$

where E_M is the bandgap energy of an unperturbed N-free host material, E_N is the energy of the localized N-level near the conduction band edge of the host material, and V_{NM} is the interaction strength between the host material conduction band and the N-level. In this model we have modified the BAC-model such that the strain induced bandgap shift from Eq. (8) is included in the E_g of the host material, so E_M in Eq. (9) is replaced by $(E_M + \Delta E_g)$, in a similar fashion as the effect of hydrostatic pressure has been taken into account for GaInNAs by Shan *et al.* [17] For simplicity, the small effect of strain for other BAC-model parameters has been neglected. The employed bandgap energies of binaries and BAC parameters are listed in Table 3 and Table 4, respectively.

The bandgaps of ternaries obtained from Eq. (9) are then used for calculating the E_g of quaternary GaNAsSb and InNAsSb. For these alloys a change in the N fraction y affects both the As and Sb fractions, and hence the N fraction should be divided proportionally between the As and Sb fractions. Therefore, the Sb fraction z is replaced by $z' = z + yz/(1 - y)$ [25,27]. Now the bandgaps of GaNAsSb and InNAsSb are approximated in the form of a quadratic function [25]:

$$\begin{cases} E_{g,GaNAsSb} = (1-z')E_{g,GaNAs} + z'E_{g,GaNSb} - z'(1-z')C_{GaNAsSb}, \\ E_{g,InNAsSb} = (1-z')E_{g,InNAs} + z'E_{g,InNSb} - z'(1-z')C_{InNAsSb}, \end{cases} \quad (10)$$

where C is the quaternary related bowing parameter describing the deviation from a linear interpolation. Finally using the bandgaps of the quaternaries, the E_g of the GaInNAsSb alloy is estimated using a similar quadratic formula:

$$E_{g,GaInNAsSb} = (1-x)E_{g,GaNAsSb} + xE_{g,InNAsSb} - x(1-x)C_{GaInNAsSb}, \quad (11)$$

where the bowing parameter C is now dependent on the In, N and Sb compositions. The composition dependent empirical bowing parameter for GaInNAsSb is given in a polynomial form:

$$C_{GaInNAsSb} = c_1x^2 + c_2x + c_3y^2 + c_4y + c_5z^2 + c_6z + c_7, \quad (12)$$

where c_1-c_7 are fitted parameters.

The model was then fitted with the experimental composition and bandgap data by employing differential evolution (DE) algorithm [28]. The parameters used for fitting were the bowing parameters for GaNAsSb and InNAsSb in Eq. (10), and parameters c_1-c_7 used in Eq. (12) to describe the composition dependency of the bowing parameter. The model parameters obtained from the DE fitting are given in Table 5.

The bandgap energies predicted by the model as function of the measured E_g data are plotted in Fig. 2. The datapoints align closely to the ideal line with an average deviation of only 12 meV between the predicted and measured E_g values. The maximum deviation within the dataset was 36 meV. In this composition region the calculated E_g values do not exhibit any significant systematic drift from the measured E_g values with respect to In, N or Sb compositions. This is illustrated by Fig. 3, which shows the ratio between calculated E_g and measured E_g as function of In, N and Sb compositions. In addition, the data in Fig. 3 shows that all the datapoints predicted by the model are within ±5% from the measured values of E_g, further demonstrating the accuracy of the proposed model. The deviation between the predicted and measured E_g was also analyzed statistically. Normalized frequency distribution as function of the difference between calculated and measured bandgap values is shown in Fig. 4. The frequency distribution of the deviation within the dataset shows that over 50% of the datapoints are within ±10 meV of the measured bandgap energies and 96% of the datapoints are within ±30 meV of the corresponding experimental E_g values. The data in Fig. 4 also indicates that the predicted values tend to be slightly more on the negative side, meaning that the model slightly underestimates the E_g of the GaInNAsSb alloys. Yet this deviation is relatively small, which can be seen from the normal distribution fitted for the experimental data points describing the deviation of an expanded dataset. The mean of the fitted distribution is at −3.5 meV and the standard deviation is only 14.3 meV. Outside the composition range of the samples analyzed in this work ($0 \le x \le 0.17$, $0 \le y \le 0.08$, $0 \le z \le 0.08$) the accuracy of the model might deteriorate, and the model parameters might require further refinement.

In conclusion, a novel interpolation method based on the BAC-modelling for predicting E_g of bulk dilute nitride GaInNAsSb compounds was introduced. The model utilizing the bowing parameters fitted with differential evolution algorithm exhibits an excellent correlation with the experimental E_g values in a relatively broad composition range ($0 \le x \le 0.17$, $0 \le y \le 0.08$, $0 \le z \le 0.08$), which includes the

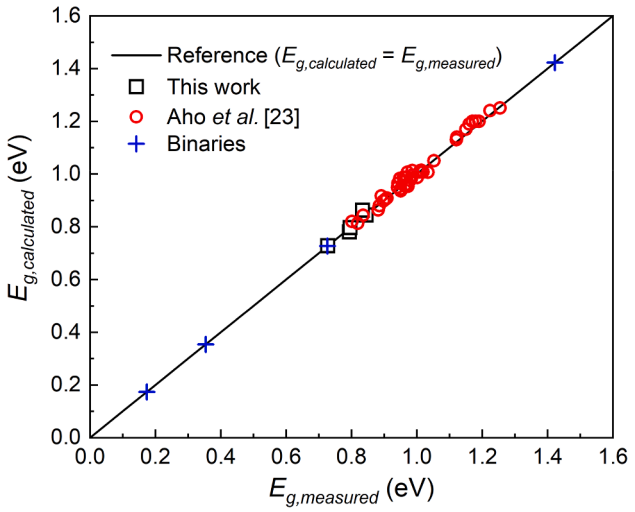

Fig. 2. Calculated bandgap energies as function of measured E_g values. The reference line represents a case where the calculated E_g is equal with the measured E_g. The black squares are datapoints based on the additional high-N GaInNAsSb samples presented in this work, the red circles are datapoints based on data by Aho *et al.*[23], while the blue crosses represent N-free binary compounds (GaAs, GaSb, InAs and InSb).

Table 5
Fitted values for $C_{GaNAsSb}$, $C_{InNAsSb}$ and parameters c_1-c_7 used to calculate the composition dependent bowing parameter of GaInNAsSb.

$C_{GaNAsSb}$ (eV)	$C_{InNAsSb}$ (eV)	c_1 (eV)	c_2 (eV)	c_3 (eV)	c_4 (eV)	c_5 (eV)	c_6 (eV)	c_7 (eV)
0.70	7.38	−0.26	13.2	283.7	−50.0	132.2	−13.7	−0.35

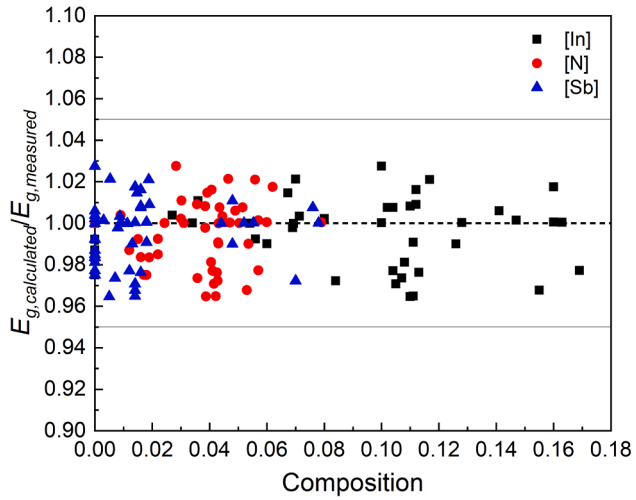

Fig. 3. Ratio between calculated E_g and measured E_g as function of In, N and Sb compositions. The dashed horizontal line shows the ideal fit, and the solid horizontal lines show the ±5% deviation from the measured bandgap energies.

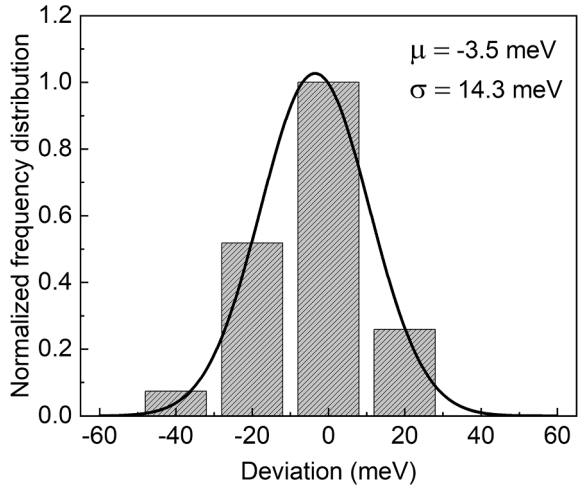

Fig. 4. Normalized frequency distribution of deviation between the E_g values predicted by the model and the and measured E_g values. The solid line represents a fitted normal distribution for an expanded dataset. The mean for the normal distribution of the expanded dataset is −3.5 meV and the standard deviation is 14.3 meV.

high-N containing alloys (up to 8%) especially relevant for development of next-generation multijunction solar cells. Furthermore, the model includes the effect of strain. The average deviation between the estimated and measured E_g values was only 12 meV. We consider the model to be a simple and effective tool in epitaxy for accurately predicting bandgaps of GaInNAsSb alloys prior to crystal growth, thus helping in the process for material composition calibration and structure design.

Declaration of Competing Interest

The authors declare that they have no known competing financial interests or personal relationships that could have appeared to influence the work reported in this paper.

Acknowledgements

The financial support provided by the European Research Council (ERC AdG AMETIST, #695116) is acknowledged. The work is also part of the Academy of Finland Flagship Program PREIN #320168. R. I. acknowledges financial support received from HPY Research Foundation.

References

[1] M. Weyers, M. Sato, H. Ando, Red shift of photoluminescence and absorption in dilute GaAsN alloy layers, Jpn. J. Appl. Phys. 31 (Part 2, No. 7A) (1992) L853–L855.
[2] M. Kondow, K. Uomi, A. Niwa, T. Kitatani, S. Watahiki, Y. Yazawa, GaInNAs: A novel material for long-wavelength-range laser diodes with excellent high-temperature performance, Jpn. J. Appl. Phys. 35 (1996) 1273–1275.
[3] J.S. Harris, GaInNAs long-wavelength lasers: progress and challenges, Semicond. Sci. Technol. 17 (8) (2002) 880–891.
[4] G. Steinle, H.D. Wolf, M. Popp, A.Y. Egorov, G. Kristen, H. Riechert, Novel monolithic VCSEL devices for datacom applications, in: 2001 Proceedings. 51st Electronic Components and Technology Conference (Cat. No. 01CH37220), 2001, 218-222.
[5] A. Ramakrishnan, G. Steinle, D. Supper, C. Degen, G. Ebbinghaus, Electrically pumped 10 Gbit/s MOVPE-grown monolithic 1.3 μm VCSEL with GaInNAs active region, Electron. Lett. 38 (2002) 322–324.
[6] Y.Q. Wei, M. Sadeghi, S.M. Wang, P. Modh, A. Larsson, High performance 1.28 μm GaInNAs double quantum well lasers, Electron. Lett. 41 (2005) 1328–1330.
[7] M. Dumitrescu, M. Wolf, K. Schulz, Y.Q. Wei, G. Adolfsson, J. Gustavsson, J. Bengtsson, M. Sadeghi, S. Wang, A. Larsson, J. Lim, E. Larkins, P. Melanen, P. Uusimaa, M. Pessa, 10 Gb/s uncooled dilute-nitride optical transmitters operating at 1.3 μm, 2009 Conference on Optical Fiber Communication, 2009, 1–3.
[8] V. Sabnis, H. Yuen, M. Wiemer, High-efficiency multijunction solar cells employing dilute nitrides, AIP Conf. Proc. 1477 (2012) 14–19.
[9] M.A. Green, K. Emery, Y. Hishikawa, W. Warta, E.D. Dunlop, Solar cell efficiency tables (version 41), Prog. Photovolt.: Res. Appl. 21 (2013) 1–11.
[10] A. Tukiainen, A. Aho, G. Gori, V. Polojärvi, M. Casale, E. Greco, R. Isoaho, T. Aho, M. Raappana, R. Campesato, M. Guina, High-efficiency GaInP/GaAs/GaInNAs solar cells grown by combined MBE-MOCVD technique, Prog. Photovolt. Res. Appl. 24 (7) (2016) 914–919.
[11] A. Aho, R. Isoaho, L. Hytönen, T. Aho, M. Raappana, V. Polojärvi, A. Tukiainen, J. Reuna, S. Mäkelä, M. Guina, Lattice-matched four-junction tandem solar cell including two dilute nitride bottom junctions, Prog. Photovolt. Res. Appl. 27 (4) (2019) 299–305.
[12] R. Isoaho, A. Aho, A. Tukiainen, T. Aho, M. Raappana, T. Salminen, J. Reuna, M. Guina, Photovoltaic properties of low-bandgap (0.7–0.9 eV) lattice-matched GaInNAsSb solar junctions grown by molecular beam epitaxy on GaAs, Sol. Energy Mater. Sol. Cells 195 (2019) 198–203.
[13] A. Aho, A. Tukiainen, V. Polojärvi, J. Salmi, M. Guina, High current generation in dilute nitride solar cells grown by molecular beam epitaxy, in: Proc. SPIE 8620, Physics, Simulation, and Photonic Engineering of Photovoltaic Devices II. (2013) 86201I.
[14] M. Guina, S.M. Wang, A. Aho, Chapter 5 - Molecular Beam Epitaxy of Dilute Nitride Optoelectronic Devices, in: M. Henini (Ed.), Molecular Beam Epitaxy (Second Edition), Elsevier, 2018, pp. 73–94.
[15] J. Wu, W. Shan, W. Walukiewicz, Band anticrossing in highly mismatched III–V semiconductor alloys, Semicond. Sci. Technol. 17 (2002) 860–869.
[16] I. Vurgaftman, J.R. Meyer, L.R. Ram-Mohan, Band parameters for III–V compound semiconductors and their alloys, J. Appl. Phys. 89 (11) (2001) 5815–5875.
[17] W. Shan, W. Walukiewicz, J.W. Ager, E.E. Haller, J.F. Geisz, D.J. Friedman, J. M. Olson, S.R. Kurtz, Band Anticrossing in GaInNAs Alloys, Phys. Rev. Lett. 82 (6) (1999) 1221–1224.
[18] I. Vurgaftman, J.R. Meyer, Band parameters for nitrogen-containing semiconductors, J. Appl. Phys. 94 (6) (2003) 3675–3696.
[19] W. Walukiewicz, K. Alberi, J. Wu, W. Shan, K.M. Yu, J.W. Ager, Electronic Band Structure of Highly Mismatched Semiconductor Alloys, in: A. Erol (Ed.), Dilute III-V Nitride Semiconductors and Material Systems: Physics and Technology, Springer, Berlin Heidelberg, Berlin, Heidelberg, 2008, pp. 65–89.
[20] E.P. O'Reilly, A. Lindsay, P.J. Klar, A. Polimeni, M. Capizzi, Trends in the electronic structure of dilute nitride alloys, Semicond. Sci. Technol. 24 (2009), 033001.
[21] V. Polojärvi, E.-M. Pavelescu, A. Schramm, A. Tukiainen, A. Aho, J. Puustinen, M. Guina, Optical properties and thermionic emission in solar cells with InAs quantum dots embedded within GaNAs and GaInNAs, Scr. Mater. 108 (2015) 122–125.
[22] Y.T. Lin, T.C. Ma, T.Y. Chen, H.H. Lin, Energy gap reduction in dilute nitride GaAsSbN, Appl. Phys. Lett. 93 (2008), 171914.
[23] A. Aho, V.-M. Korpijärvi, R. Isoaho, P. Malinen, A. Tukiainen, M. Honkanen, M. Guina, Determination of composition and energy gaps of GaInNAsSb layers grown by MBE, J. Cryst. Growth 438 (2016) 49–54.

[24] M. Gladysiewicz, R. Kudrawiec, M.S. Wartak, Theoretical studies of optical gain tuning by hydrostatic pressure in GaInNAs/GaAs quantum wells, J. Appl. Phys. 115 (2014), 033515.
[25] R. Kudrawiec, Conduction and valence band positions versus the Fermi-level stabilization energy in quaternary dilute nitrides, Phys. Status Solidi C. 8 (5) (2011) 1650–1654.
[26] P.H. Jefferson, T.D. Veal, L.F.J. Piper, B.R. Bennett, C.F. McConville, B.N. Murdin, L. Buckle, G.W. Smith, T. Ashley, Band anticrossing in GaNxSb1−x, Appl. Phys. Lett. 89 (2006), 111921.
[27] R. Kudrawiec, Parameterization of the band gap energy for GaNxAs1−x−zPz alloys, J. Appl. Phys. 101 (2007), 116101.
[28] M. Wormington, C. Panaccione, K.M. Matney, D.K. Bowen, Characterization of structures from X-ray scattering data using genetic algorithms, Phil. Trans. R. Soc. A. 357 (1761) (1999) 2827–2848.